

SPACE-CLIP: Spatial Perception via Adaptive CLIP Embeddings for Monocular Depth Estimation

Taewan Cho, Taeryang Kim, and Andrew Jaeyong Choi

Abstract—Contrastive Language-Image Pre-training (CLIP) provides strong semantic representations, but it is not designed for dense geometric prediction. Most CLIP-based monocular depth methods still rely on text prompts and image-text matching, which adds indirection and inference overhead. We propose SPACE-CLIP, a decoder-only framework that predicts depth directly from a frozen CLIP vision encoder and fully bypasses the text encoder. Its decoder fuses scene-level context from FiLM-conditioned semantic features with fine spatial cues from shallow layers. Under the TFI-FB constraint (text-free inference and frozen vision backbone), SPACE-CLIP achieves AbsRel 0.0901 on KITTI and 0.1042 on NYU Depth V2. These results, together with ablations, show that hierarchical fusion of semantic and structural cues is effective while preserving modularity for embodied AI systems such as vision-language-action (VLA) models. We also observe stable training behavior across both datasets with the same frozen-backbone setting, which supports reproducible deployment in integration-constrained pipelines. Our model is available at <https://github.com/taewan2002/space-clip>

Index Terms—Monocular depth estimation, Contrastive Language-Image Pre-training (CLIP), Vision-Language Models, Foundation models, Computer vision.

I. INTRODUCTION

Large-scale vision-language models (VLMs), such as CLIP [1], have advanced semantic visual understanding. In parallel, monocular depth estimation remains a core problem for 3D scene understanding in applications such as autonomous driving and augmented reality [2]. Unlike recognition tasks, monocular depth estimation requires dense geometric reasoning and precise local structure. This mismatch makes direct reuse of CLIP non-trivial.

Prediction quality is only part of the problem. Many high-performing depth estimators are task-specific and computationally heavy, which increases latency and complicates integration in larger multimodal systems. In VLA models, adding a separate depth stack can also duplicate visual encoders and create brittle interfaces. Recent lightweight VLA results also indicate that preserving spatial context under strict compute budgets is critical for downstream control performance [3]. As illustrated in Figure 1, this motivates a practical question: can we design a depth module that is both accurate and architecturally compatible with agentic systems?

Early CLIP-based depth methods usually follow a prompt-and-match strategy: they query CLIP with text prompts (e.g., “a photo of a car far away”) or fine-tune the image encoder.

Taewan Cho, Taeryang Kim, and Andrew Jaeyong Choi are with the School of Computing, Gachon University, Republic of Korea (e-mail: {taewan2002, ktr1110, andrewjchoi}@gachon.ac.kr).

Corresponding author: Andrew Jaeyong Choi (andrewjchoi@gachon.ac.kr).

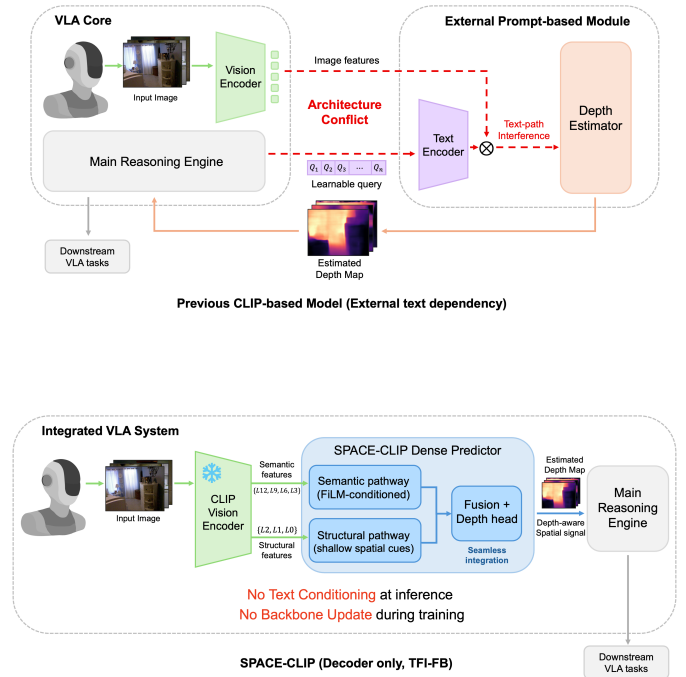


Fig. 1. VLA integration challenge and the SPACE-CLIP solution. SPACE-CLIP adds a decoder-only spatial head to a shared frozen vision backbone and avoids text-path interference.

Prompt-based routes struggle to represent continuous depth with discrete language, while full fine-tuning increases compute and can harm pre-trained representations. This trade-off leads to a direct question: can we decode latent geometric cues from a foundation model without modifying its core parameters?

We answer this question with SPACE-CLIP, which shifts depth estimation from prompt-and-match to direct interpretation. As shown in Figure 2, the model uses a dual-pathway decoder that extracts and fuses semantic and structural signals from a frozen CLIP vision encoder while bypassing the text encoder. The semantic pathway uses deeper CLIP layers and FiLM [4] to inject global context. The structural pathway uses shallow layers to preserve local geometric detail.

Under the TFI-FB constraint, SPACE-CLIP achieves AbsRel 0.0901 on KITTI [5] and 0.1042 on NYU Depth V2 [6]. Frozen visual features can support geometric prediction when paired with a compact decoder. This modular design fits multimodal systems, including VLA models.

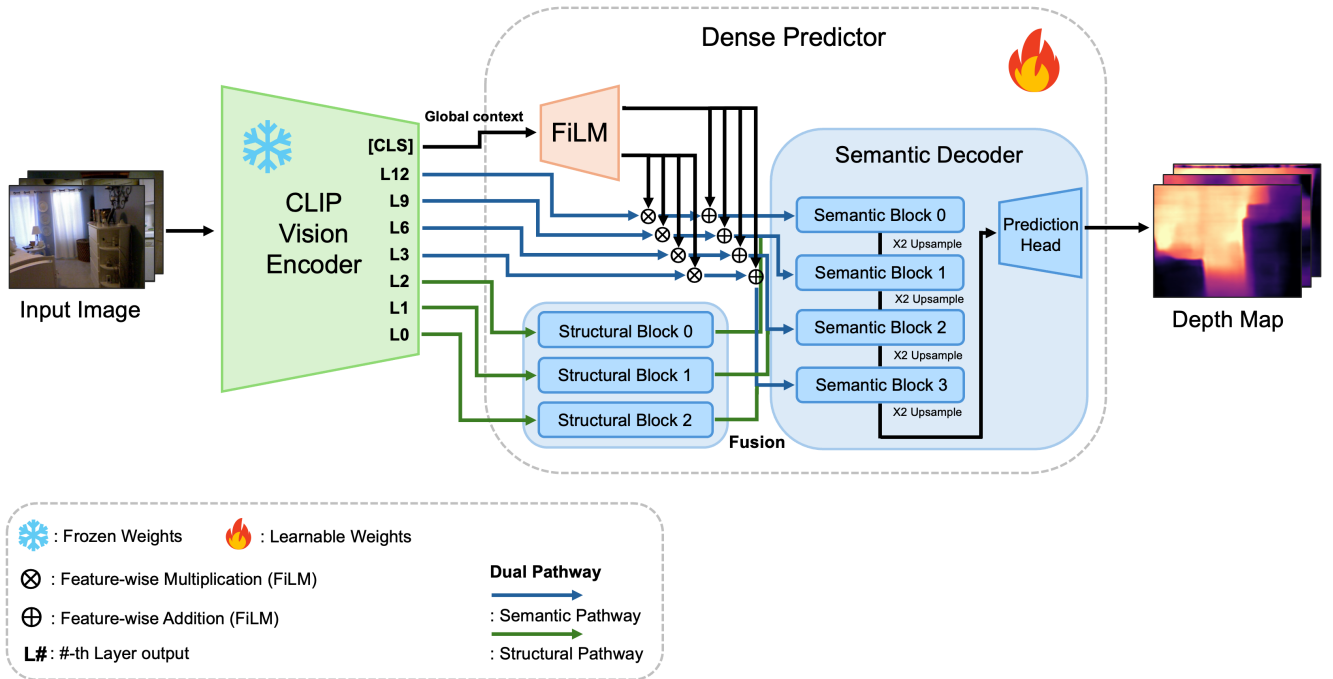


Fig. 2. Overall architecture of SPACE-CLIP. A frozen CLIP encoder feeds a dual-pathway dense predictor, and semantic/structural features are fused hierarchically for depth prediction.

II. RELATED WORK

A. Monocular Depth Estimation

Monocular depth estimation has progressed from CNN encoder-decoder models to Transformer- and SSM-based designs. Early CNN methods established strong supervised baselines but often lost boundary detail due to repeated downsampling [7]. Later work improved feature fusion and objectives, including ordinal regression in DORN [8] and improved losses [9].

Transformer-based methods improved long-range reasoning. DPT [10] showed that ViT backbones can outperform strong CNN baselines. Follow-up works such as DepthFormer [11], ASTRansformer [12], and NeWCRFs [13] further improved performance through specialized architectural choices. More recently, MambaDepth [14] explored state-space modeling for efficient long-range dependency capture.

Recent foundation-model directions emphasize cross-domain generalization at scale. Depth Anything and Depth Anything V2 leverage large-scale pseudo-labeled training for robust monocular depth prediction [15], [16]. UniDepth targets universal metric depth across domains with camera-aware modeling [17], while Metric3Dv2 focuses on zero-shot metric depth and surface normal estimation across diverse camera settings [18]. More recently, Depth Anything at Any Condition extends this line toward condition-aware depth estimation under challenging degradations and weather conditions [19]. Complementary studies in Neurocomputing report transformer fusion, uncertainty modeling, and multimodal cues for depth estimation [20]–[22], as well as earlier self-/unsupervised

monocular depth objectives [23], [24]. Neurocomputing also reports related advances in geometry-aware monocular perception and robot learning under continual adaptation constraints [25], [26].

These specialized models define a strong performance frontier, but they are often less modular for integration into larger multimodal systems. Our work targets this integration setting by keeping the backbone frozen and moving adaptation into a compact decoder.

B. Vision-Language Models for Dense Prediction

Large-scale VLMs such as CLIP opened new directions for depth estimation. Prior work mainly follows two routes: prompt engineering for depth querying and architectural adaptation of vision encoders.

1) *Advancements in Prompt Engineering for Depth:* Prompt-centered methods ask how to query CLIP for depth. DepthCLIP [27] used fixed prompts such as “close” and “far,” but discrete language is a weak representation of continuous geometry. Later work introduced learnable or adaptive prompts. Auty et al. [28] replaced human-defined words with continuous tokens; CaBins [29] generated prompts from image features; Hu et al. [30] used scene-dependent codebooks; and CLIP2Depth [31] used mirror embeddings. Despite these improvements, these methods remain tied to text encoding and image-text matching.

2) *Architectural Adaptation of Vision Encoders:* Another line of work adapts CLIP vision encoders for dense prediction. For example, CaBins [29] modifies the image pathway for

richer multi-scale features. However, prediction still depends on prompt-mediated image-text alignment.

SPACE-CLIP removes this dependency. We hypothesize that high-level semantics and low-level structure are already encoded hierarchically in frozen visual features. Our adaptation target is the decoder, which maps visual features directly to depth without any text-encoder path.

III. METHOD

SPACE-CLIP decodes latent geometric information from a frozen CLIP vision encoder. As shown in Figure 2, the pipeline has three stages: (1) multi-level feature extraction from the frozen CLIP encoder, (2) parallel semantic and structural decoding, and (3) hierarchical fusion for high-fidelity depth prediction.

The full system predicts high-resolution depth maps, while the CLIP branch input is generated by bicubic resizing to 224×224 (not center cropping). This keeps the frozen backbone interface fixed and delegates high-resolution reconstruction to the decoder.

A. Overall Architecture

Our design principle is modularity. By freezing the large CLIP backbone and training only a compact decoder, SPACE-CLIP can serve as a perception plugin in larger agents without modifying their base vision encoder.

We use pre-trained CLIP ViT-B/16 as the frozen backbone. The learnable module is the Dense Predictor, which takes multi-level hidden states from CLIP.

As shown in Figure 2, the Dense Predictor has two pathways: a Semantic Pathway and a Structural Pathway. The semantic stream models scene-level context, while the structural stream preserves low-level spatial detail. Their outputs are fused hierarchically during decoding to produce depth maps that are globally coherent and locally precise.

B. Dual Pathway Feature Processing

The Dense Predictor processes features by abstraction level and assigns different CLIP layers to each pathway.

1) *Semantic Pathway with FiLM*: The semantic pathway uses deep CLIP layers (L12, L9, L6, and L3), which encode abstract scene-level information but have lower spatial fidelity.

To improve context-aware decoding, we use Feature-wise Linear Modulation (FiLM) [4]. Global context is extracted from the final [CLS] token. A small MLP maps this vector v_{cls} to channel-wise scale and shift parameters γ and β , which modulate each semantic patch feature F_{patch} :

$$\text{FiLM}(F_{patch}, \gamma, \beta) = \gamma \cdot F_{patch} + \beta \quad (1)$$

This conditioning adapts local feature interpretation to global scene context.

2) *Structural Pathway*: The structural pathway uses shallow CLIP layers (L2, L1, and L0), which preserve high-resolution cues such as edges and textures.

We do not apply FiLM in this pathway, so geometric detail is not entangled with semantic modulation. Structural blocks refine these features before fusion with the semantic stream.

C. Hierarchical Fusion Decoder

SPACE-CLIP uses staged fusion rather than independent decoding. The decoder progressively upsamples features, and each stage concatenates the upsampled semantic representation with the corresponding structural feature.

As shown in Figure 2, each semantic block is followed by $2 \times$ upsampling. Matching structural features provide high-frequency detail that the semantic stream lacks. This creates a coarse-to-fine refinement process: semantic features provide global layout, while structural features recover boundaries and local detail. A final prediction head outputs the high-resolution depth map.

D. Loss Function

Loss design is important in depth estimation because it controls how spatial relations are learned from supervision [32]. We train SPACE-CLIP with a composite objective that balances scale-invariant accuracy and local structural consistency. The total loss is:

$$\mathcal{L}_{\text{total}} = (1 - \lambda_{\text{ssim}})\mathcal{L}_{\text{SILog}} + \lambda_{\text{ssim}}\mathcal{L}_{\text{SSIM}} \quad (2)$$

where $\lambda_{\text{ssim}} = 0.5$.

1) *Scale-Invariant Logarithmic (SILog) Loss*: SILog focuses on relative depth structure rather than absolute scale, which suits monocular ambiguity. For predicted depth \hat{d} and ground truth depth d , we define $g_i = \log(\hat{d}_i) - \log(d_i)$ over N valid pixels. SILog is:

$$\mathcal{L}_{\text{SILog}}(\hat{d}, d) = \alpha \sqrt{\frac{1}{N} \sum_i g_i^2 - \frac{\lambda}{N^2} \left(\sum_i g_i \right)^2} \quad (3)$$

We set $\lambda = 0.85$ and $\alpha = 10$.

2) *Structural Similarity (SSIM) Loss*: SILog captures relational depth accuracy but does not directly enforce local structural consistency. We therefore add SSIM loss, which compares luminance, contrast, and structure between predicted and ground-truth depth maps. For two windows x and y :

$$\text{SSIM}(x, y) = \frac{(2\mu_x\mu_y + C_1)(2\sigma_{xy} + C_2)}{(\mu_x^2 + \mu_y^2 + C_1)(\sigma_x^2 + \sigma_y^2 + C_2)} \quad (4)$$

where μ and σ denote mean and standard deviation, and C_1, C_2 are stabilizing constants. We compute SSIM loss as the mean of $(1 - \text{SSIM})$.

IV. EXPERIMENTS

A. Datasets

We evaluated on KITTI [5] and NYU Depth V2 [6]. KITTI represents outdoor driving scenes, while NYU Depth V2 represents indoor scenes. For KITTI, we used the standard Eigen split: For KITTI, we followed the standard Eigen split with approximately 22,600 training images from 32 scenes and 697 test images from 29 non-overlapping scenes, using LiDAR-derived depth supervision. For NYU Depth V2, we followed the standard train/test protocol used in prior monocular depth estimation work. In our setup, we resized KITTI images to

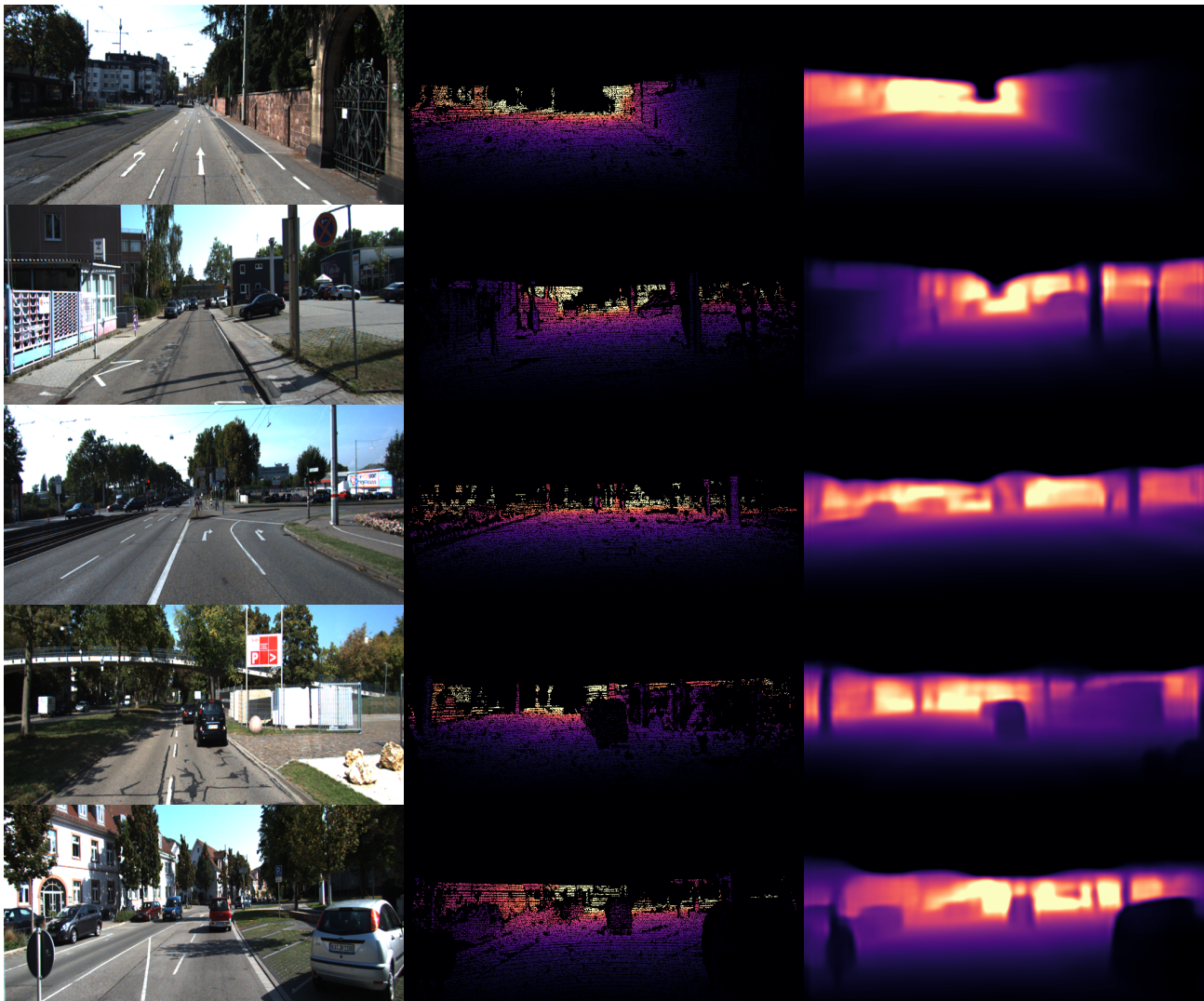


Fig. 3. Qualitative comparison on KITTI. From left to right: input image, ground truth, and SPACE-CLIP prediction. The model reconstructs detailed depth maps for thin poles, distant vehicles, and foliage.

352×704 for depth prediction and generated the CLIP input by bicubic resizing to 224×224 . We applied random horizontal flips and random rotations up to 1.0 degree.

B. Implementation Details

1) *Model and Architecture*: For all runs, we used the pre-trained ViT-B/16 CLIP model [33] (openai/clip-vit-base-patch16). We fully froze the CLIP vision encoder. All trainable parameters were in the Dense Predictor, including the FiLM generators and the semantic and structural decoders. Semantic layer indices were [12, 9, 6, 3], and structural layer indices were [2, 1, 0]. Decoder channels were [256, 128, 64, 32] with dropout 0.1 in residual blocks.

2) *Training Setup*: We trained our model in PyTorch on a single NVIDIA GPU. We used AdamW with an initial learning rate of 1×10^{-4} and weight decay 0.01. We used cosine warmup, trained for 20 epochs, and fixed random seed 42. The loss combined SILog and SSIM with $\lambda_{\text{ssim}} = 0.5$, and

we added multi-scale auxiliary SILog with weights [0.10, 0.05, 0.00]. We used EMA with decay 0.996 and selected the checkpoint by comparing raw and EMA validation results (eval_both_for_best=true). For evaluation, we used final-only flip TTA (final_eval_flip_tta=true, eval_flip_tta=false). We also applied gradient clipping with max norm 1.0.

C. Comparison with State-of-the-Art

Table I compares SPACE-CLIP with prior methods on KITTI (Eigen split). We report standard error metrics (AbsRel, SqRel, RMSE, RMSE log; lower is better) and accuracy metrics ($\delta < 1.25$, $\delta < 1.25^2$, $\delta < 1.25^3$; higher is better). Constraint labels are N/A (non-CLIP method), TC-FB (text-conditioned inference with frozen vision backbone), TC-BU (text-conditioned inference with backbone updates), and TFI-FB (text-free inference with frozen vision backbone). Non-ours rows are reported from their original papers and should be read as contextual comparisons. For consistency, our metrics are reported to four decimal places throughout the paper.



Fig. 4. Qualitative results on NYU Depth V2. From left to right: input image, ground-truth depth, and SPACE-CLIP prediction. The model captures overall geometry in indoor scenes while retaining major object boundaries.

Recent CLIP-based methods such as CaBins and CLIP2Depth achieve strong performance, often with text conditioning at inference or backbone updates during training. Recent large-scale depth foundation models (e.g., Depth Anything V2, UniDepth, and Metric3Dv2) prioritize broad zero-shot metric generalization with large-scale training pipelines [16]–[18]. By contrast, we evaluate SPACE-CLIP

under the TFI-FB constraint. Under this setting, our model remains competitive and clearly improves over earlier prompt-based baselines such as DepthCLIP and Auty et al. For example, AbsRel decreases by about 70.6% versus Auty et al. (0.307 to 0.0901).

These results support our design choice: direct decoding from frozen visual features can deliver practical geometric per-

TABLE I
PERFORMANCE COMPARISON ON KITTI (EIGEN SPLIT, 0–80 M). LOWER IS BETTER FOR ERROR METRICS, AND HIGHER IS BETTER FOR δ ACCURACY METRICS.

Method	Approach	Constraint	AbsRel↓	SqRel↓	RMSE↓	RMSE log↓	$\delta < 1.25^\dagger$	$\delta < 1.25^{2\dagger}$	$\delta < 1.25^{3\dagger}$
DORN [8]	Unimodal	N/A	0.072	0.307	2.727	0.120	0.932	0.984	0.994
ASTransformer [12]	Unimodal	N/A	0.058	-	2.685	0.089	0.963	0.995	0.999
DepthFormer [11]	Unimodal	N/A	0.052	0.158	2.143	0.079	0.975	0.997	0.999
NeWCRFs [13]	Unimodal	N/A	0.052	0.155	2.129	0.079	0.974	0.997	0.999
DepthCLIP [27]	CLIP-based	TC-FB	0.473	6.007	12.958	-	0.281	0.531	0.696
Hu <i>et al.</i> [30]	CLIP-based	TC-BU	0.384	4.661	12.290	-	0.312	0.569	0.739
Auty <i>et al.</i> [28]	CLIP-based	TC-FB	0.307	2.197	6.405	0.121	0.548	0.826	0.935
CLIP2Depth [31]	CLIP-based	TC-FB	0.074	0.303	2.948	-	0.938	0.990	0.998
CaBins [29]	CLIP-based	TC-BU	0.057	0.186	2.322	0.088	0.964	0.995	0.999
SPACE-CLIP (Ours)	CLIP-based	TFI-FB	0.0901	0.4701	3.8451	0.1528	0.9088	0.9812	0.9945

ception with a compact module. A performance gap remains to heavily specialized models, but the strict-constraint setting remains practically relevant for integration.

Following the quantitative results, we provide a qualitative comparison in Fig. 3. The figure showcases several challenging scenarios from the KITTI test set.

D. Cross-Dataset Evaluation on NYU Depth V2

To complement KITTI, Table II reports results on NYU Depth V2. Following prior work, we list unimodal and CLIP-based methods together. We take non-ours baseline numbers from the NYU comparison table in CaBins [29]; † indicates reimplementations in that source and follows the source protocol (typically standard NYU crop). We use the same constraint labels as in Table I. Our row reports the TFI-FB setting with no NYU crop in both training and evaluation (`do_nyu_crop=false`, `do_nyu_crop_eval=false`), so this table should be interpreted as contextual reference rather than strict ranking.

To complement Table II, Fig. 4 presents qualitative NYU examples. SPACE-CLIP recovers global room layout and major object boundaries, while some thin structures and small high-frequency details remain oversmoothed.

E. Ablation Studies

We ran ablations on KITTI to isolate the effect of each architectural component. Specifically, we tested FiLM-based semantic conditioning and the structural pathway. Table III summarizes the results. Rows 1–3 show controlled ablations, and row 4 reports SPACE-CLIP with both components enabled.

1) *Baseline Model*: Row 1 is the baseline: frozen CLIP encoder with a semantic-only decoder (layers 12, 9, 6, 3), without FiLM and without the structural pathway.

2) *Effect of FiLM*: Row 2 adds FiLM to the baseline by conditioning semantic patch features on global context from the [CLS] token. This gives consistent but moderate gains, including AbsRel improvement from 0.1165 to 0.1142.

3) *Effect of the Structural Pathway*: Row 3 adds the structural pathway without FiLM. This yields a larger gain (AbsRel 0.1165 to 0.1094), showing that shallow CLIP layers provide important geometric detail for boundary quality.

4) *Synergistic Effect of Both Components*: Row 4 corresponds to SPACE-CLIP with both FiLM and the structural pathway enabled, and reports AbsRel 0.0901 and RMSE 3.8451. This indicates complementarity: structural features provide local fidelity, and FiLM provides scene-level context for consistent interpretation.

V. DISCUSSION

This section interprets the empirical findings, discusses system-level implications, and outlines limitations and future directions.

A. Interpretation of Results

The ablation results in Table III support our core hypothesis: depth-relevant information is hierarchically distributed in CLIP features. Shallow layers provide fine geometric detail, while deep layers provide semantic context. FiLM alone gives modest gains, the structural pathway alone gives larger gains, and combining both gives the best results. This pattern indicates that semantic context and structural detail are complementary.

The SOTA comparison in Table I highlights a trade-off between modularity and peak task specialization. Methods that update backbones or rely on text pathways can reach stronger benchmark scores, but they are less modular and often harder to integrate into larger multimodal systems. SPACE-CLIP prioritizes frozen-backbone adaptation and still improves strongly over earlier CLIP-based baselines under comparable constraints.

B. A Blueprint for Modular Perception in Embodied AI

The main value of SPACE-CLIP is architectural: it offers a modular blueprint for spatial perception in embodied AI. Modern VLAs need robust spatial cues, but integrating monolithic depth estimators is often inefficient. Two issues are common:

TABLE II
PERFORMANCE COMPARISON ON NYU DEPTH V2. NON-OURS ROWS ARE FROM CABINS [29]; † DENOTES REIMPLEMENTATION IN THAT SOURCE.

Method	Approach	Constraint	AbsRel↓	RMSE↓	log 10↓	$\delta < 1.25\uparrow$	$\delta < 1.25^2\uparrow$	$\delta < 1.25^3\uparrow$
Make3D (reported in [29])	Unimodal	N/A	0.349	1.214	-	0.447	0.745	0.897
DORN [8]	Unimodal	N/A	0.115	0.509	0.051	0.828	0.965	0.992
ASTransformer [12]	Unimodal	N/A	0.103	0.374	0.044	0.902	0.985	0.997
DepthFormer [11]	Unimodal	N/A	0.096	0.339	0.041	0.921	0.989	0.998
NeWCRFs [13]	Unimodal	N/A	0.095	0.334	0.041	0.922	0.992	0.998
DepthCLIP [27]	CLIP-based	TC-FB	0.388	1.167	0.156	0.394	0.683	0.851
Hu <i>et al.</i> [30]	CLIP-based	TC-BU	0.347	1.049	0.140	0.428	0.732	0.898
Auty† [28]	CLIP-based	TC-FB	0.324	0.961	0.127	0.473	0.779	0.921
CaBins [29]	CLIP-based	TC-BU	0.120	0.401	0.050	0.866	0.978	0.996
SPACE-CLIP (Ours)	CLIP-based	TFI-FB	0.1042	0.3848	0.0446	0.8958	0.9839	0.9973

TABLE III
ABLATION ON KITTI FOR FiLM AND STRUCTURAL PATHWAY COMPONENTS. ✓ INDICATES AN ENABLED COMPONENT.

#	Model Configuration	FiLM	Struct. Path	AbsRel↓	SqRel↓	RMSE↓	RMSE log↓	$\delta < 1.25\uparrow$	$\delta < 1.25^2\uparrow$	$\delta < 1.25^3\uparrow$
1	Baseline			0.1165	0.7981	5.152	0.1962	0.858	0.963	0.988
2	Baseline + FiLM	✓		0.1142	0.7684	5.121	0.1941	0.862	0.964	0.988
3	Baseline + Structural Pathway		✓	0.1094	0.7238	5.143	0.1911	0.870	0.966	0.989
4	SPACE-CLIP (Ours)	✓	✓	0.0901	0.4701	3.8451	0.1528	0.9088	0.9812	0.9945

- **Architectural Conflict:** A VLA already includes a primary vision encoder for semantic understanding. Adding another depth-specific backbone introduces redundancy and inefficiency.
- **Input Interference:** Many models rely on textual prompts, which can interfere with the VLA’s own language processing pipeline.

SPACE-CLIP addresses these issues through the **TFI-FB constraint** (text-free inference and frozen vision backbone), as shown in Table I:

- 1) **Shared Backbone Principle:** SPACE-CLIP is a compact decoder-only module that can attach to an existing frozen CLIP-compatible vision encoder.
- 2) **No Textual Interference:** It bypasses the text encoder, so it does not consume or perturb the language pathway.
- 3) **Constrained Adaptation Scope:** Additional model adaptation is confined to the decoder side under TFI-FB.

This principle can extend beyond depth estimation to other dense prediction tasks, such as segmentation and surface normal estimation, by decoding hierarchical features from frozen foundation backbones. In robotics, RetoVLA shows that reusing internal tokens can improve spatial reasoning in lightweight VLA policies under strict compute limits [3]. SPACE-CLIP provides a complementary advantage: it keeps the CLIP image encoder frozen and removes text conditioning at inference, so geometric cues can be injected as a decoder-side plugin without modifying shared VLM parameters. This design choice lowers integration risk and makes joint use with

token-reuse VLA architectures a practical next step. Related evidence also appears in language-model adaptation, where DARE-based merging improves benchmark performance without full-model retraining [34].

For reproducibility, we keep three fixed settings across KITTI and NYU: TFI-FB evaluation, bicubic 224×224 CLIP input without center cropping, and checkpoint selection via raw/EMA validation comparison.

C. Limitations and Future Work

Despite promising results, our work has several limitations.

First, a performance gap remains relative to specialized vision-only models. Future work may reduce this gap with lightweight adapters in the frozen encoder or richer cross-path fusion (e.g., cross-attention) in the decoder.

Second, although we report both KITTI and NYU Depth V2, the NYU table includes a protocol mismatch (source baselines with standard crop vs. our no-crop setting), so direct ranking claims are limited.

Third, we do not yet provide standardized efficiency evidence (parameter count, FLOPs, latency/FPS, and memory) under unified hardware and batch settings. Current modularity/efficiency discussion is therefore architectural, not a benchmark claim.

Finally, we validate only on CLIP and have not yet completed downstream robotics integration or robustness analysis under adverse conditions (e.g., nighttime, rain, and strong motion blur). Future work will apply the same decoder design to other foundation models, such as DINOv2 [35], test

policy-learning impact (e.g., Diffusion Policy [36]) in VLA pipelines such as RoboMamba [37] and RetoVLA [3], and combine Register-Token context streams with SPACE-CLIP depth embeddings while preserving the frozen-backbone, text-free TFI-FB constraint.

VI. CONCLUSION

We introduced SPACE-CLIP, a text-free monocular depth model that reads geometric cues directly from a frozen CLIP vision encoder. The decoder combines FiLM-conditioned semantic context with a structural branch that preserves local detail. Under the TFI-FB constraint, SPACE-CLIP reaches AbsRel 0.0901 on KITTI and 0.1042 on NYU Depth V2 in our evaluation setting, and ablations show that each branch contributes while the joint design performs best. This result indicates that frozen foundation features can support modular depth estimation when adaptation remains in a compact decoder. The next step is to pair this design with standardized efficiency measurements and downstream VLA integration tests so that modularity gains are quantified at the system level.

ACKNOWLEDGMENT

This work was supported by the Gachon University research fund(GCU-202500670001).

REFERENCES

- [1] A. Radford, J. W. Kim, C. Hallacy, A. Ramesh, G. Goh, S. Agarwal, G. Sastry, A. Askell, P. Mishkin, J. Clark *et al.*, "Learning transferable visual models from natural language supervision," in *International conference on machine learning*. PmLR, 2021, pp. 8748–8763.
- [2] K. Dhanushkodi, A. Bala, and N. Chaplot, "Single-view depth estimation: Advancing 3d scene interpretation with one lens," *IEEE Access*, vol. 13, pp. 20 562–20 573, 2025.
- [3] J. Koo, T. Cho, H. Kang, E. Pyo, T. G. Oh, T. Kim, and A. J. Choi, "Retovla: Reusing register tokens for spatial reasoning in vision-language-action models," 2025. [Online]. Available: <https://arxiv.org/abs/2509.21243>
- [4] E. Perez, F. Strub, H. De Vries, V. Dumoulin, and A. Courville, "Film: Visual reasoning with a general conditioning layer," in *Proceedings of the AAAI conference on artificial intelligence*, vol. 32, no. 1, 2018.
- [5] A. Geiger, P. Lenz, C. Stiller, and R. Urtasun, "Vision meets robotics: The kitti dataset," *International Journal of Robotics Research (IJRR)*, 2013.
- [6] P. K. Nathan Silberman, Derek Hoiem and R. Fergus, "Indoor segmentation and support inference from rgb-d images," in *ECCV*, 2012.
- [7] X. Yang, Q. Chang, X. Liu, S. He, and Y. Cui, "Monocular depth estimation based on multi-scale depth map fusion," *IEEE Access*, vol. 9, pp. 67 696–67 705, 2021.
- [8] H. Fu, M. Gong, C. Wang, K. Batmanghelich, and D. Tao, "Deep ordinal regression network for monocular depth estimation," in *Proceedings of the IEEE conference on computer vision and pattern recognition*, 2018, pp. 2002–2011.
- [9] S. F. Bhat, I. Alhashim, and P. Wonka, "Adabins: Depth estimation using adaptive bins," in *Proceedings of the IEEE/CVF Conference on Computer Vision and Pattern Recognition (CVPR)*, June 2021, pp. 4009–4018.
- [10] R. Ranftl, A. Bochkovskiy, and V. Koltun, "Vision transformers for dense prediction," in *Proceedings of the IEEE/CVF international conference on computer vision*, 2021, pp. 12 179–12 188.
- [11] Z. Li, Z. Chen, X. Liu, and J. Jiang, "Depthformer: Exploiting long-range correlation and local information for accurate monocular depth estimation," *Machine Intelligence Research*, vol. 20, no. 6, pp. 837–854, 2023.
- [12] W. Chang, Y. Zhang, and Z. Xiong, "Transformer-based monocular depth estimation with attention supervision," in *BMVC*, vol. 6, 2021, p. 7.
- [13] W. Yuan, X. Gu, Z. Dai, S. Zhu, and P. Tan, "Neural window fully-connected crfs for monocular depth estimation," in *Proceedings of the IEEE/CVF conference on computer vision and pattern recognition*, 2022, pp. 3916–3925.
- [14] I. Grigore and C.-A. Popa, "Mambadepth: Enhancing long-range dependency for self-supervised fine-structured monocular depth estimation," *arXiv preprint arXiv:2406.04532*, 2024.
- [15] L. Yang, B. Kang, Z. Huang, X. Xu, J. Feng, and H. Zhao, "Depth anything: Unleashing the power of large-scale unlabeled data," *arXiv preprint arXiv:2401.10891*, 2024.
- [16] L. Yang, B. Kang, Z. Huang, Z. Zhao, X. Xu, J. Feng, and H. Zhao, "Depth anything v2," *arXiv preprint arXiv:2406.09414*, 2024.
- [17] L. Piccinelli, C. Sakaridis, M. Segu, Y. Li, L. Van Gool, and F. Yu, "Unidepth: Universal monocular metric depth estimation," in *Proceedings of the IEEE/CVF Conference on Computer Vision and Pattern Recognition (CVPR)*, June 2024, pp. 12 613–12 623.
- [18] Y. Hu, Z. Yang, B. Lu, G. Xiao, S. Yi, Y. Wu, Z. Zhou, Z. Cui, Y. Shen, X. Shen *et al.*, "Metric3dv2: A versatile monocular geometric foundation model for zero-shot metric depth and surface normal estimation," *arXiv preprint arXiv:2312.11584*, 2024.
- [19] L. Yang, B. Kang, Z. Huang, Z. Yang, X. Xu, J. Feng, and H. Zhao, "Depth anything at any condition," *arXiv preprint arXiv:2507.01634*, 2025.
- [20] P. Liu, Z. Zhang, Z. Meng, and N. Gao, "Transformer-based monocular depth estimation with hybrid attention fusion and progressive regression," *Neurocomputing*, vol. 620, p. 129268, 2025.
- [21] Y. Zhu, R. Ren, W. Dong, X. Li, and G. Shi, "Tsudepth: Exploring temporal symmetry-based uncertainty for unsupervised monocular depth estimation," *Neurocomputing*, vol. 600, p. 128165, 2024.
- [22] X. Huang, Y. Ma, Z. Yu, and H. Zhao, "Redformer: Transformer-based dense depth estimation by sparse radar and camera," *Neurocomputing*, vol. 589, p. 127668, 2024.
- [23] M. Zhang, X. Ye, X. Fan, and W. Zhong, "Unsupervised depth estimation from monocular videos with hybrid geometric-refined loss and contextual attention," *Neurocomputing*, vol. 379, pp. 250–261, 2020.
- [24] L. Chen, W. Tang, T. R. Wan, and N. W. John, "Self-supervised monocular image depth learning and confidence estimation," *Neurocomputing*, vol. 381, pp. 272–281, 2020.
- [25] X. Wu, D. Ma, X. Qu, X. Jiang, and D. Zeng, "Depth dynamic center difference convolutions for monocular 3d object detection," *Neurocomputing*, vol. 520, pp. 73–81, 2023.
- [26] W. Liu, W. Yao, K. Yang, L. Ren, and C. Sun, "Overcoming catastrophic forgetting in robotic manipulation via knowledge-compositional reinforcement learning," *Neurocomputing*, vol. 664, p. 131800, 2026.
- [27] R. Zhang, Z. Zeng, Z. Guo, and Y. Li, "Can language understand depth?" in *Proceedings of the 30th ACM International Conference on Multimedia*, 2022, pp. 6868–6874.
- [28] D. Auty and K. Mikolajczyk, "Learning to prompt clip for monocular depth estimation: Exploring the limits of human language," in *Proceedings of the IEEE/CVF International Conference on Computer Vision (ICCV) Workshops*, October 2023, pp. 2039–2047.
- [29] E. Son and S. J. Lee, "Cabins: Clip-based adaptive bins for monocular depth estimation," in *Proceedings of the IEEE/CVF Conference on Computer Vision and Pattern Recognition*, 2024, pp. 4557–4567.
- [30] X. Hu, C. Zhang, Y. Zhang, B. Hai, K. Yu, and Z. He, "Learning to adapt clip for few-shot monocular depth estimation," in *Proceedings of the IEEE/CVF Winter Conference on Applications of Computer Vision*, 2024, pp. 5594–5603.
- [31] D. Kim and S. Lee, "Clip can understand depth," *arXiv preprint arXiv:2402.03251*, 2024.
- [32] F. Khan, S. Hussain, S. Basak, M. Moustafa, and P. Corcoran, "A review of benchmark datasets and training loss functions in neural depth estimation," *IEEE Access*, vol. 9, pp. 148 479–148 503, 2021.
- [33] A. Dosovitskiy, L. Beyer, A. Kolesnikov, D. Weissenborn, X. Zhai, T. Unterthiner, M. Dehghani, M. Minderer, G. Heigold, S. Gelly *et al.*, "An image is worth 16x16 words: Transformers for image recognition at scale," *arXiv preprint arXiv:2010.11929*, 2020.
- [34] T. Cho, R. Kim, and A. J. Choi, "Research on enhancing model performance by merging with korean language models," *Engineering Applications of Artificial Intelligence*, vol. 159, p. 111686, 2025. [Online]. Available: <https://www.sciencedirect.com/science/article/pii/S0952197625016884>
- [35] M. Oquab, T. Darcet, T. Moutakanni, H. Vo, M. Szafraniec, V. Khalidov, P. Fernandez, D. Haziza, F. Massa, A. El-Nouby *et al.*, "Dinov2: Learning robust visual features without supervision," *arXiv preprint arXiv:2304.07193*, 2023.

- [36] C. Chi, Z. Xu, S. Feng, E. Cousineau, Y. Du, B. Burchfiel, R. Tedrake, and S. Song, "Diffusion policy: Visuomotor policy learning via action diffusion," *The International Journal of Robotics Research*, p. 02783649241273668, 2023.
- [37] J. Liu, M. Liu, Z. Wang, L. Lee, K. Zhou, P. An, S. Yang, R. Zhang, Y. Guo, and S. Zhang, "Robomamba: Multimodal state space model for efficient robot reasoning and manipulation," *arXiv preprint arXiv:2406.04339*, 2024.